Journal of Alloys and Compounds 880 (2021) 160503

Contents lists available at ScienceDirect

Journal of Alloys and Compounds

journal homepage: www.elsevier.com/locate/jalcom

Magnesium aluminate spinel for optically stimulated luminescence dosimetry

L. Pan[a], S. Sholom[b], S.W.S. McKeever[b], L.G. Jacobsohn[a,*]

[a] Department of Materials Science and Engineering, Clemson University, 515 Calhoun Dr., Sirrine Hall #161 Clemson, SC 29634, USA
[b] Department of Physics, Oklahoma State University, Stillwater, OK, USA

ARTICLE INFO

Article history:
Received 24 March 2021
Received in revised form 17 May 2021
Accepted 20 May 2021
Available online 23 May 2021

Keywords:
Spinel
$MgAl_2O_4$
OSL
Defect
Luminescence

ABSTRACT

Motivated by the search of new materials for optically stimulated luminescence (OSL) dosimeters, magnesium aluminum spinels with different Mg:Al ratios were investigated. Powders were prepared *via* the co-precipitation method with Mg:Al ratios 1:2 (stoichiometric), 1.5:2 (MgO-rich) and 1:3 (Al_2O_3-rich) and calcined at 1000 °C in air for 2 h. A higher level of structural disorder was found in the powders than in the single crystal as determined by X-ray diffraction and Raman spectroscopy measurements, while the same luminescence centers were present in all materials as shown by X-ray induced radioluminescence measurements. Among the different Mg:Al ratios, stoichiometric spinel presented superior OSL dose response, being linear within 0.16 Gy and 2 Gy, presenting 1% reproducibility of the dosimetric response after repeated exposure to the same dose, having the least fading, and with a minimum detectable absorbed dose (MDD) of 0.65 mGy.

1. Introduction

Magnesium aluminate spinel, $MgAl_2O_4$, has a cubic crystallographic structure where oxygen ions form a nearly cubic closed pack. Since the arrangement of the oxygen ions is not perfectly cubic, the tetrahedral sites are larger while the octahedral sites are narrowed and tilted in relation to the expected perfectly cubic packing [1]. The regular unit cell has eight chemical formulae with Mg ions occupying eight of the sixty four tetrahedral sites and Al occupying sixteen of the thirty two octahedral sites. In the case of Al_2O_3-rich magnesium aluminate spinel, it has been shown that Al excess is accommodated by the creation of Al_{Mg} anti-site defects and Al vacancies for charge compensation. Up to 30% cationic disorder was observed through the partial exchange of lattice positions between Mg^{2+} and Al^{3+} [2–5]. Density functional theory calculations showed the formation of anti-site defects to be energetically more favorable than of vacancies and interstitials [6]. The Al_2O_3-MgO phase diagram reveals that non-stoichiometric ratios between MgO and Al_2O_3 lead to the formation of solid solutions and of Al_2O_3 or MgO phases, depending on the relative amounts of the parent oxides [7].

$MgAl_2O_4$ has attracted the attention of the scientific community due to its high resistance to radiation damage and potential for optical applications, in part due to its large band gap estimated to be within 7.75–8.2 eV [8–10]. In terms of ionizing radiation detection and measurement, $MgAl_2O_4$ was investigated as a scintillator under X-ray excitation when doped with Mn [11–13] as well as with diverse rare earth ions (Dy, Tb, Ce and Tm) [14–16].

Presently, there are only two commercially available optically stimulated luminescence (OSL) dosimeters, BeO and Al_2O_3:C, fabricated by Dosimetrics and Landauer, respectively. New materials are sought towards better efficiency and performance [17–21] and, within the context of OSL dosimetry, the Al_2O_3-MgO phase diagram was explored in this work. $MgAl_2O_4$ is potentially attractive for OSL dosimetry [17] due to its relatively low effective atomic number $Z_{eff} = 11.2$ that is between that of human tissue ($Z_{eff} = 7.35–7.65$) and compact bone ($Z_{eff} = 13.6$) [22]. Recently, the investigation of $MgAl_2O_4$ as an OSL dosimeter received further impulse when the material was doped with a variety of elements, including rare earths [23–26]. In magnesium aluminate spinel solid solutions, anti-site defects are formed, *i.e.*, Mg^{2+} replacing Al^{3+} and Al^{3+} replacing Mg^{2+} [2]. The replacement of an Al^{3+} ion located in a tetrahedral site with Mg^{2+} yields an electron trap, and the replacement of a Mg^{2+} ion in an octahedral site with Al^{3+} yields a hole trap. This work builds on this structural knowledge and represents a preliminary report of how different $MgO:Al_2O_3$ ratios affect the OSL behavior of this material.

* Corresponding author.
E-mail address: luiz@clemson.edu (L.G. Jacobsohn).

https://doi.org/10.1016/j.jallcom.2021.160503
0925-8388/

2. Experimental procedures

Magnesium aluminum spinel with three nominal compositions $MgAl_2O_4$·0.5MgO (MgO-rich; 1.5:2 (0.75) Mg:Al ratio), $MgAl_2O_4$ (stoichiometric; 1:2 (0.5) Mg:Al ratio) and $MgAl_2O_4$·0.5Al_2O_3 (Al_2O_3-rich; 1:3 (0.33) Mg:Al ratio) were prepared *via* the co-precipitation method. $Al(NO_3)_3$·9H_2O (Beantown Chemical, 99.999%) and $Mg(NO_3)_2$·6H_2O (Beantown Chemical, 99.95%) were used as precursors. The stoichiometric material was prepared using a 1:2 mol ratio of the precursors, 0.005 mol (1.2821 g) $Mg(NO_3)_2$·6H_2O and 0.01 mol (3.7513 g) $Al(NO_3)_3$·9H_2O, while MgO-rich was prepared with a 1.5:2 ratio and Al_2O_3-rich with a 1:3 ratio of the Mg and Al precursors. These precursors were dissolved under room temperature (RT) stirring in 30–40 mL ultrapure 18.2 MΩ water provided by a Thermo Scientific Barnstead Smart2Pure water purification system based on 0.2 µm particle and reverse osmosis filtering of prefiltered water. The total amount of water was adjusted from 30 to 40 mL to keep a 0.5 total mol/L concentration fixed: 30 mL for the 1:2 precursor ratio, 35 mL for the 1.5:2 ratio, and 40 mL for the 1:3 ratio. Once a homogenous solution was formed, ammonia (Alfa Aesar, 28 wt%) was dropwise added into the solution under vigorous stirring until pH = 11 was reached. The resulting solution was further stirred for 30 min followed by three cycles of centrifuging and rinsing with ultrapure 18.2 MΩ water and finally dried at 80 °C overnight. Dried powders were ground and calcined at 1000 °C for 2 h in air. No further thermal treatment was executed on the powders.

X-ray diffraction (XRD) 2θ scans from 10° to 80° at a rate of 0.5°/min were executed with a Rigaku Ultima IV X-ray diffractometer with Cu Kα radiation (40 kV, 40 mA). All samples were in powder form.

Raman backscattering spectroscopy was performed with a Horiba LabRAM HR Evolution confocal microscope equipped with an 800 mm focal length spectrograph and an air-cooled (−60 °C) back-illuminated deep-depleted 1024 × 256 pixels CCD detector. A 100 mW frequency doubled Nd:YAG laser emitting at 532 nm, 50% neutral density filter, 50× magnification objective, and 600 groves/mm diffraction grating were used in the measurements. Spectra corresponded to the average of ten 20 s-long scans. Spectra were corrected by the pre-recorded instrument-specific response to a calibrated white light source, namely the intensity correction system (ICS). A $MgAl_2O_4$ (100) single crystal acquired from MSE Supplies, LLC, was used as reference.

Radioluminescence (RL) measurements were executed using a customer-designed configuration of the Freiberg Instruments Lexsyg Research spectrofluorometer equipped with a Varian Medical Systems VF-50J X-ray tube with a tungsten target [27]. The X-ray source was coupled with an ionization chamber for continuous radiation intensity monitoring. The light emitted by the sample was collected by an Andor Technology SR-OPT-8024 optical fiber connected to an Andor Technology Shamrock 163 spectrograph coupled to a cooled (−80 °C) Andor Technology DU920P-BU Newton CCD camera (spectral resolution ~ 0.5 nm/pixel). RL was measured under continuous X-ray irradiation (40 kV, 1 mA) at RT. Integration time was 50 s for the powders and 10 s for the single crystal. Powders filled *ca.* 8 mm diameter 0.5 mm deep cups thus allowing for relative RL intensity comparison between different samples. RL was also measured as a function of temperature with an integration time of 5 s while continuously heating the sample to 400 °C with a heating rate of 1 °C/s. Spectra were corrected by the built-in wavelength response of the system.

Continuous-wave (CW) mode OSL was measured with an automated Risø TL/OSL-DA-15 reader with a blue light emitting diode (LED; centered at 470 nm) for sample stimulation and a bialkali EMI 9235QB photomultiplier tube for detection using a Hoya U-340 glass filter (transmittance: 260–390 nm). Samples were exposed to different doses in the 0.16–80 Gy range using an internal Risø $^{90}Sr/^{90}Y$ beta source with a dose rate of ~ 0.08 Gy/s. The mass of the samples was between 16.8 mg and 19.3 mg. OSL curves were recorded for different stimulation times and analyzed by a combination of independent exponential decay functions, in addition to one free constant background: $I_{OSL}(t) = \sum_j A_j e^{-t/\tau_j} + A_0$, where A_j and τ_j are an the initial intensity and the time constant of the decay curve j, respectively, and A_0 is the background. The fractional contribution of the time constants f_i was calculated based on the following equation: $f_i = \frac{A_i \tau_i}{\sum_j A_j \tau_j}$ [28].

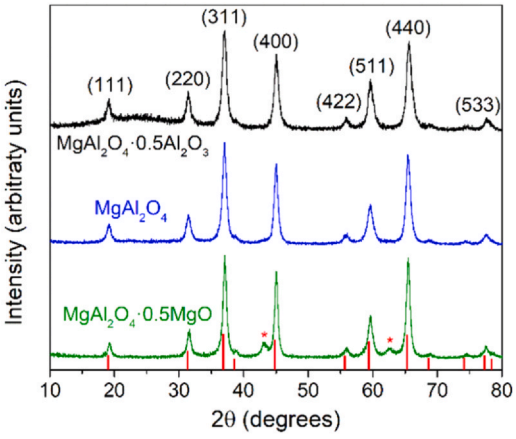

Fig. 1. XRD results of magnesium aluminate spinels synthesized with different Mg:Al ratios where the most intense diffraction peaks were labeled according to JCPDS 21-1152 that corresponds to stoichiometric MgAl2O4 (red bars). The asterisks indicate a MgO secondary phase. Diffractograms were vertically shifted to enhance visual clarity.

3. Results and discussion

3.1. XRD

XRD results are shown in Fig. 1 together with JCPDS PDF card #21-1152 (bar plot) that corresponds to cubic stoichiometric $MgAl_2O_4$ where the major diffraction peaks were labeled. The presence of a secondary phase of cubic MgO (indicated by *) according to JCPDS PDF card #45-0946 was only observed in the MgO-rich material. In the case of the Al_2O_3-rich material, the presence of an amorphous phase was revealed by the broad band centered at 2θ ~ 25°.

3.2. Raman spectroscopy

Raman backscattering spectroscopy results are presented in Fig. 2 together with the spectrum obtained from a $MgAl_2O_4$ (100) single crystal as a reference. The single crystal presented the following peaks: 222 cm^{-1} ascribed to the translation of Al^{3+} in a tetrahedral site, 305 cm^{-1} (T_{2g}) ascribed to the translation of Mg^{2+} in a tetrahedral site, 404 cm^{-1} (E_g) related to internal vibrations of Al^{3+} in a octahedral site, 485 cm^{-1} (T_{2g}), 663 cm^{-1} (T_{2g}) related to internal vibrations of Al^{3+} in a octahedral site, and 764 cm^{-1} (A_{1g}) related to the symmetric Mg–O stretching vibration in a tetrahedral site. The 720 cm^{-1} (A_{1g}) peak was related to the symmetric Al–O stretching vibration in a tetrahedral site but also attributed to phonons that become active in the disordered structure due to coupling with the Mg–O vibration in a tetrahedral site [29–32]. All the Raman peaks observed in the single crystal spectrum were also observed in the powders, with those from the powders being broader and thus indicative of the presence of some level of structural disorder. However, the powders presented additional peaks (marked by arrows in Fig. 2) at about 570 cm^{-1} and as a low frequency unresolved shoulder to the 404 cm^{-1} peak. The shoulder was attributed to the bending

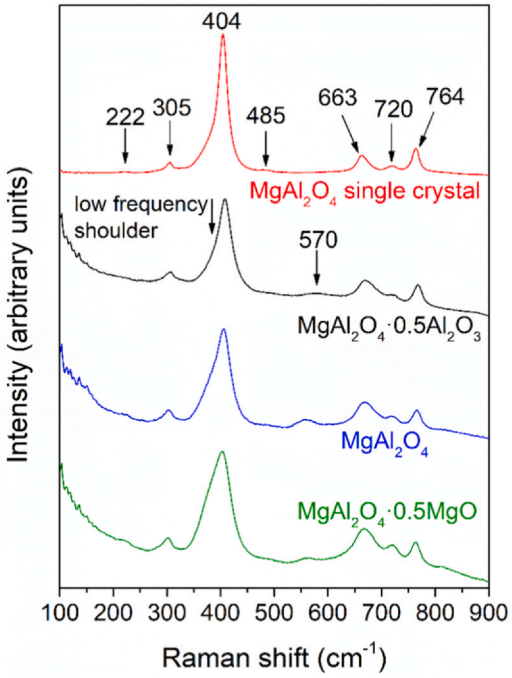

Fig. 2. Raman backscattering spectroscopy results of magnesium aluminate spinels with different Mg:Al ratios together with those from a $MgAl_2O_4$ (100) single crystal. Peak positions are indicated in cm^{-1}. Spectra were vertically shifted to enhance visual clarity.

mode of Al^{3+} in tetrahedral sites [31], while the 570 cm^{-1} peak possibly to an Al-related bending mode [30]. As per the above discussion, peaks at 222 cm^{-1} and 720 cm^{-1} and the low frequency shoulder to peak at 404 cm^{-1} are related to structural disorder. Relative intensity analysis of the 222 cm^{-1} peak showed them to be more intense in the powders than in the single crystal. In the case of the low frequency shoulder, its relative intensity to the 404 cm^{-1} peak was considerably more intense for the stoichiometric and MgO-rich materials than for the single crystal. Consequently, it was concluded that while exchange of Al^{3+} and Mg^{2+} was present even in the single crystal, exchange disorder was considerably higher in the powders.

3.3. Radioluminescence

RL spectra of spinels with different Mg:Al ratios together with the spectrum of the single crystal are reported in Fig. 3. They revealed the presence of several emission bands within the 230–750 nm spectral range: a broad band centered at 400 nm, a narrow band at 515 nm and an intense narrow band peaked at 687 nm composed of a series of weaker peaks at 674 nm, 698 nm, 708 nm and 717 nm that became progressively less resolved for increasing Mg:Al ratios. Excluding the single crystal that presented significantly higher RL intensity, and besides the 515 nm band, all other bands had essentially the same intensity regardless the Mg:Al ratio. Also, an increase of the background above about 700 nm was observed for progressively higher Mg:Al ratios.

The intrinsic luminescence of $MgAl_2O_4$ is composed of many emission bands and while it has been the subject of many reports, it is not free of controversy. This complexity is understood, at least in part, due to a broad range of cationic disorder favored by the low energy of formation of anti-site defects [6] that is difficult to properly characterize, and to the efficient luminescence of transition metals, even when present at trace levels. Below, a critical summary of the literature is presented.

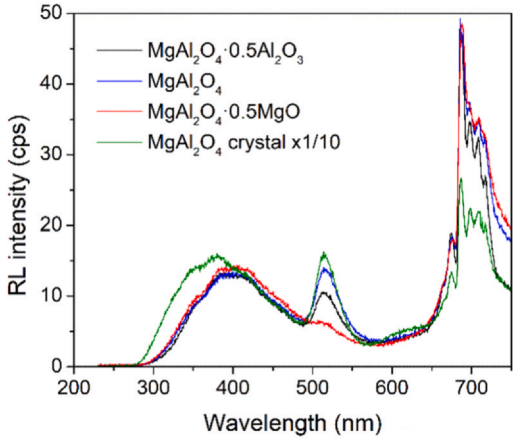

Fig. 3. RL spectra of magnesium aluminate spinels with different Mg:Al ratios together with that from a $MgAl_2O_4$ (100) single crystal. The spectrum of the single crystal was divided by a factor of 10.

Under ultraviolet and X-ray excitation, nominally stoichiometric and Mg-deficient as well as nominally pure and transition metal-doped (Mn, Cr, Fe, Zn) $MgAl_2O_4$ emits a broad emission at about 710–750 nm [7,33–36] and at about 650 nm [7,34,36]. These emissions have been attributed to color centers related to a Mg vacancy [35]. The set of fine peaks around the 687 nm peak have been attributed to Cr^{3+} impurities in octahedral sites [37,38] and emission at 517 nm to Mn^{2+} incorporated in tetrahedral sites in stoichiometric $MgAl_2O_4$ [38]. The latter peak emission wavelength increased linearly (within a narrow spectral range of ~ 8 nm) for higher Mg:Al ratios from 0.3 to 1 [36].

An emission band observed at 461 nm under excitation at 234 nm has been attributed to F centers [39] because the excitation band is where the absorption band of F centers is expected based on Mollwo-Ivey [40] and thermochemical [41] analyses. However, an excitation band at 261 nm has also been attributed to F^+ centers based on similarities of the F to F^+ conversion process in Al_2O_3 [8] and excitation at 264 nm yields emission around 460 nm. The latter work concluded that the 460 nm emission was from F^+ centers due to the photoionization of F centers, the excited state of which lies close to the bottom of the conduction band [42]. Aside from the controversy over the identification of the specific defect that originates luminescence, the underpinning relationship of these bands to cationic vacancies seems clear.

A broad emission band at about 400 nm has sometimes been observed [37,43–45] and shown that it could be excited at 275 nm [44]. To date, its origin has not been identified.

An emission band at 335 nm has been attributed to intracenter transitions in anti-site defects [9 and references therein] but has also been tentatively attributed to F^+ centers, albeit without supporting arguments [46].

An intense complex band at about 250 nm that, in fact, corresponds to the superposition of two bands at about 245 nm and 275 nm, has also been commonly reported. These bands have been attributed to electron-hole recombination at V-type centers with Mg'_{Al} anti-site defects serving as the hole center [10,37,43,47,48]. We note that the 250 nm band has only been observed in stoichiometric and Al_2O_3-rich magnesium aluminate spinels [33], and published reports indicate that neutron [9] and ion irradiation [10], as well as the incorporation of transition metals (Mn, Cr, Fe) [49], considerably decrease or even fully suppress this emission.

In order to gain further insight into the nature of the emission bands present in our spinels, Gaussian spectral analysis was performed from 2.2 eV to 5 eV, including a $MgAl_2O_4$ single crystal as reference. No attempt was made to fit the longer-wavelength/lower-energy region.

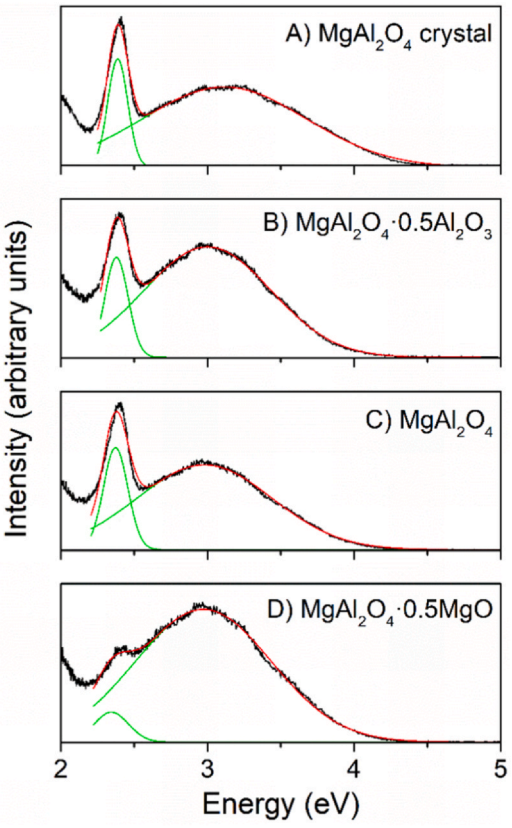

Fig. 4. Two Gaussian best-fitting of RL spectra within the 2.2–5 eV range of A) magnesium aluminate spinel single crystal and B–D) magnesium aluminate spinels with different Mg:Al ratios.

Combinations of two, three and four Gaussian bands were used to represent all or some of the bands reported in the literature within this spectral range, namely the bands at 335 nm, 400 nm, 461 nm and 515 nm. The 515 nm band was present in all fittings as evident from visual inspection of Fig. 3. For the fittings to be physically meaningful, the width of the individual Gaussian bands was limited to values ≥0.8 eV since this is a typical value for the width of luminescence bands related to structural defects at RT [46,48]. Giving its origin from Mn^{2+} ions, the 515 nm band was an exception to this rule and its width was freely adjusted. The best fitting results were obtained with only two Gaussian bands, one for the 515 nm band and the other for the 400 nm band, as shown in Fig. 4 where green curves correspond to individual Gaussian bands and red lines to the cumulative best fit. It is noted that best fits with three and four Gaussian bands (515 nm + 400 nm + either or both 335 nm and 461 nm) yielded good fits if the width constraint was relaxed to 0.7 eV. However, in the best fits using three and four Gaussian bands, the relative contribution (area) of the 335 nm and/or 461 nm bands in relation to the 400 nm band was always around 10%. These results show that even if present, the 335 nm and 461 nm bands were not intense. On the other hand, no reasonable fittings were obtained with the combination of 515 nm + 461 nm + 335 nm Gaussian bands. These results showed that while the nature of the 400 nm band remains elusive, it is important to consider its use in spectral analysis.

The results of best fits with two Gaussian bands yielded bands at 2.34–2.38 eV (530–521 nm) with width of 0.16–0.23 eV and at 2.97–3.00 eV (418–413 nm) with width of about 0.87–0.93 eV. In the case of MgO-rich material, the lower energy position at 2.34 eV (in comparison to 2.37 eV and 2.38 eV for the other spinels) and broader width (0.23 eV against 0.16 eV and 0.17 eV for the other spinels) of

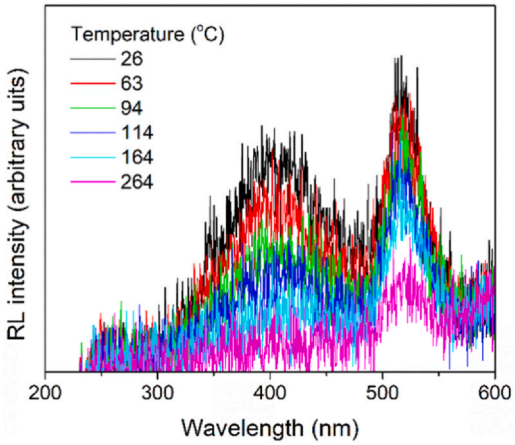

Fig. 5. Selected RL spectra of magnesium aluminate spinel synthesized with 1:2 Mg:Al (stoichiometric) ratio obtained at different temperatures.

the 515 nm band was attributed to its weak intensity together with the influence of the tail of the Cr^{3+} band at lower energies that was not included in the fitting procedure. The width of the 515 nm band is in agreement with the commonly reported width of the Mn^{2+} emission band within 0.12 eV and 0.31 eV [50]. These results are in good agreement with the analysis of the single crystal that yielded bands at 2.39 eV (519 nm) width of 0.14 eV and 3.11 eV (399 nm) with width of 1.11 eV. Further, they are supported by RL measurements of the stoichiometric spinel as a function of temperature shown in Fig. 5 for representative temperatures. Assuming that different luminescence centers have different thermal stabilities, these results suggest the presence of only two bands, one around 400 nm and the other at 515 nm.

In addition to the 400 nm and 515 nm bands there are the longer-wavelength emission bands, as shown in Fig. 3. The similarity of the position and fine structure of the band peaked at 687 nm with reports in the literature [37,38] unequivocally identified it as luminescence from Cr^{3+} in $MgAl_2O_4$. The position, shape and asymmetry of the 515 nm band observed in this work agreed with RL spectra reported for Mn-doped $MgAl_2O_4$ single crystals [11]. Also, the 515 nm band presented a small red-shift (~0.8 nm) for increasing Mg:Al ratio from 0.33 to 0.5, in agreement with a previous report on Mn-doped $MgAl_2O_4$ single crystals [36]. Moreover, the manufacturer's certificate of analysis confirmed that the Mg nitrate hexahydrate precursor contained 32 ppm Mn (the Al nitrate nonahydrate precursor contained <1 ppm Mn). The above facts are strong evidence for the attribution of the 515 nm band to Mn^{2+} impurities. However, the intensity of the 515 band did not follow the Mg:Al ratio since it nearly vanished for the MgO-rich spinel. This is explained by the formation of a MgO phase exclusively in the MgO-rich spinel and that Mn^{2+} RL emission in MgO occurs at 760 nm [51]. Indeed, the emission background above 700 nm is highest for the MgO-rich material. The background emission above 700 nm observed in this work is thus attributed to color centers related to Mg vacancies in $MgAl_2O_4$ according to [35], and in the case of the MgO-rich sample, also to Mn^{2+} luminescence in the MgO secondary phase [51].

The results of the spectral analysis are indicative of the absence of, or small concentrations of, the defects related to the 335 nm band, *i.e.*, anti-site defects or F^+ centers, and of the band at 461 nm attributed to F or F^+ centers. On the other hand, strong evidence for the defect related to the 400 nm band was obtained. Further, no emission was observed below ~ 300 nm. It has been reported in the literature that when the 400 nm band is dominant, the 250 nm band is missing altogether [33,37,43,45,46,48,49,52]. The current data are consistent with these observations.

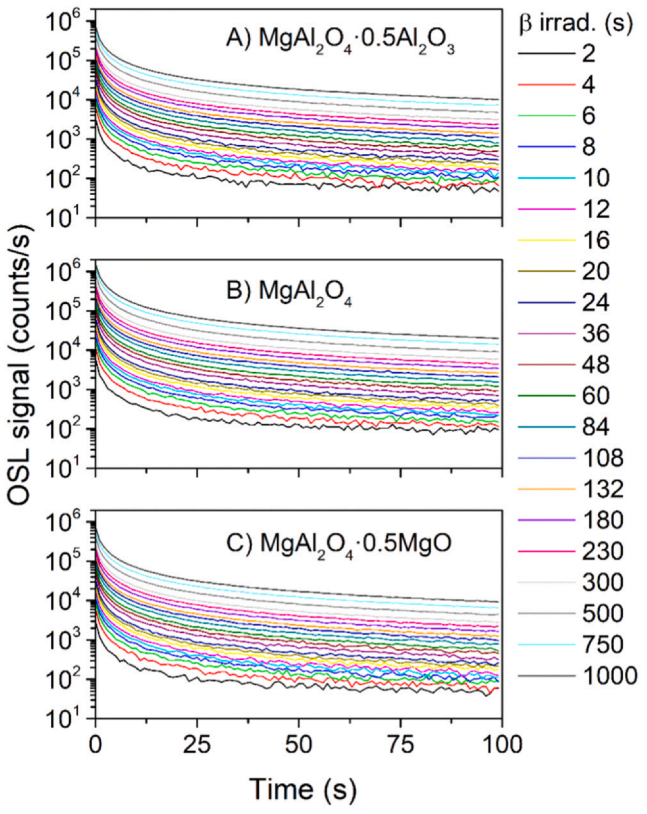

Fig. 6. OSL curves of spinels with different Mg:Al ratios obtained after different irradiation times indicated in the color legend, in seconds. All figures are in the same scale to facilitate comparison.

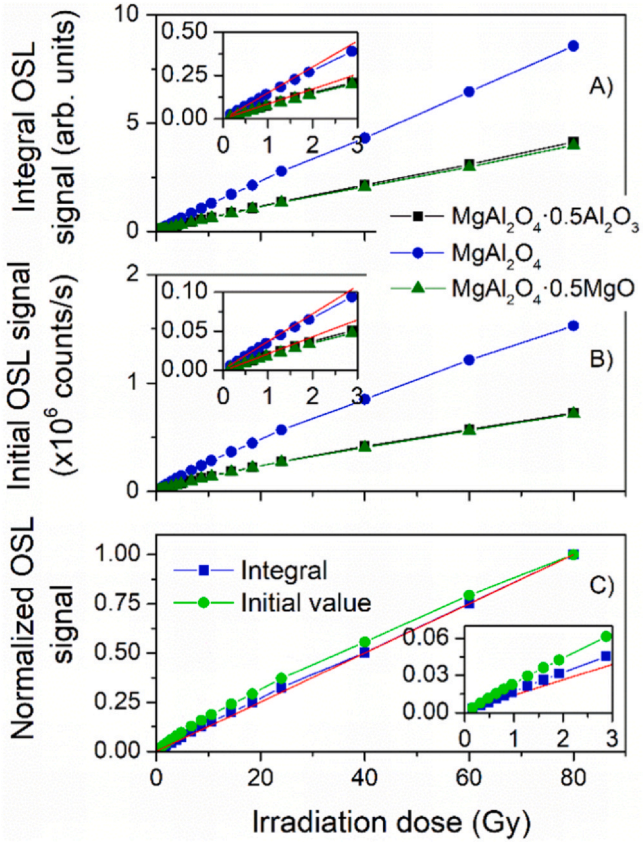

Fig. 7. Linearity of the OSL dose response based on the OSL integral (A) and initial value (B) of spinels with different Mg:Al ratios. Figure (C) compares the normalized integral and initial value dose responses of the stoichiometric spinel, together with a straight line that serves reference. The insets present a close-up to the OSL response to doses up to 3 Gy. The red straight lines are guides to the eye to highlight non-linearity effects.

3.4. Optically stimulated luminescence

The results of the investigation of OSL properties of magnesium aluminate spinel with different Mg:Al ratios are presented in Figs. 6–10. It is noted that only emission within 260–390 nm was recorded due to the use of the filter Hoya U-340. Consequently, based on RL results (cf. Figs. 3–5), the OSL results are related to the luminescence center(s) responsible for the 400 nm band discussed previously. In Fig. 6, the OSL dose response for irradiation times from 2 s (0.16 Gy) to 1000 s (80 Gy) and illumination time up to 100 s are presented in the same scale to facilitate comparison. Overall, the same behavior was observed in all spinels with the intensity of the OSL signal increasing with irradiation time. The degree of linearity of the dose response was evaluated in terms of the OSL integral value ($1\ s \le t \le 100\ s$) and the OSL initial value ($t = 1\ s$) as shown in Fig. 7A and B, respectively. While these results indicated an apparent trend toward saturation for all spinels, the behavior is tentatively attributed to fading during irradiation. Over lower doses when the irradiation times were shorter the dose-response curves are more linear (cf. insets in Fig. 7A and B) with stoichiometric spinel showing less deviation from linearity than the other spinels. Two OSL measurements were evaluated, namely the initial OSL value (OSL intensity after 1 s of stimulation) and the total OSL signal (summation of OSL signal from $t = 1$ to 100 s). These are compared in Fig. 7C where the results are normalized to the respective highest value. Clearly, the integral signal delivered a more linear response as highlighted in the inset of Fig. 7C. The range of linearity of the stoichiometric spinel was from 0.16 Gy to ~2 Gy for the integral approach and only up to ~1 Gy for the initial value approach.

The minimum detectable absorbed dose (MDD) was determined using OSL curves of samples irradiated in the dose range of 0.16–1.28 Gy. The MDD was defined as that dose that corresponded to a signal equal to 3-times the standard deviation of the background, the background being defined as the OSL intensity within the 90–100 s range of stimulation time. These results are summarized in Table 1 and revealed the MDD of the stoichiometric spinel to be 0.65 mGy that was about half of the MDD value of the non-stoichiometric spinels.

Reproducibility of the OSL response was evaluated by seven sequential cycles of 10 s irradiation/readout of the same sample for each Mg:Al ratio for a total stimulation time of 600 s. The average initial value (at $t = 1$ s) of the stoichiometric material was 1.9× and 2.2 × higher than the Al_2O_3-rich and MgO-rich spinels, respectively. The standard deviation of the initial value obtained from these seven independent measurements was around 1% of the respective average value. Reproducibility was also evaluated for the initial 10 s integral signal and for the background that corresponded to the average over the last 10 s of the curve. These results are presented in Fig. 8A for all three Mg:Al ratios where they were normalized by the initial OSL signal (Fig. 8A) and initial background signal (Fig. 8B) measured after the first irradiation (cycle #1) of the respective sample. The stoichiometric spinel showed a variation within ~1% that is acceptable for dosimetric applications. Interestingly, the background showed a decreasing trend for higher irradiation/readout cycles, reaching a

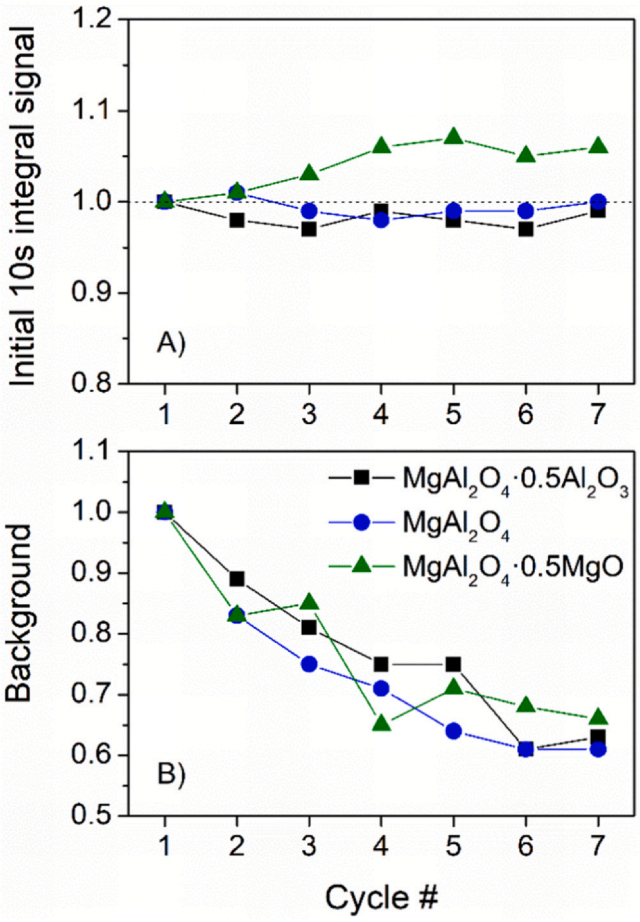

Fig. 8. Initial 10 s integral signal (A) and background (B) values obtained from spinels with different Mg:Al ratios after the indicated number of measurement/irradiation cycles. See text for details.

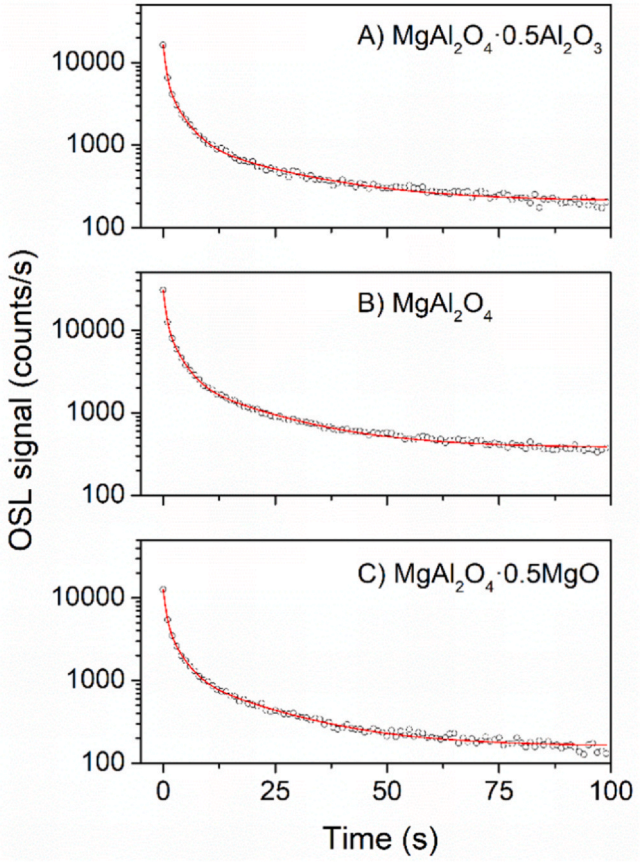

Fig. 9. OSL curves obtained after 100 s stimulation of spinels with different Mg:Al ratios (open circles) together with best fit using three exponential functions (red lines) and one free constant background. Samples were irradiated for 10 s. All figures are in the same scale to facilitate comparison.

decrease down to 60–70% of the original background signal after the seventh cycle (Fig. 8B). This behavior was tentatively attributed to a very long-lived, hard-to-bleach signal. The fact that the background was sensitive to the irradiation history remains an issue that will need to be accounted for in practical applications of $MgAl_2O_4$ in OSL dosimetry. Overall, these observations revealed the stoichiometric spinel to be superior in performance than the non-stoichiometric spinels.

OSL curves obtained over 100 s of stimulation after irradiation times of 10 s, 100 s and 200 s, and over 600 s stimulation after an irradiation time of 10 s were analyzed by the combination of independent exponential decay functions, in addition to one free constant background. The best fits for a stimulation time of 100 s were obtained by the combination of three exponential functions while for a stimulation time of 600 s needed four exponential functions. These results are illustrated in Figs. 9 and 10 for an irradiation time of 10 s while Tables 2 and 3 summarize the best fit results in terms of time constants and their fractional contributions. For the stimulation time of 100 s, the time constants were essentially the same for all spinels and irradiation times, namely *ca.* 0.6 s, 3 s, and 19 s. The OSL decay was dominated by the longest time constant (~54%) followed by the intermediate (~35%) and the shortest (~11%) time constants. For the stimulation time of 600 s, the three shortest time constants were about the same as in the 100 s case, *i.e.*, *ca.* 0.5 s, 2.5 s, 13 s, with an additional time constant of 121 s. The fractional contributions were evenly distributed among the four components, being within 21–32% (Table 3). The observation of a much longer time constant supports the interpretation of the background behavior discussed earlier (Fig. 8B). The fact that different irradiation times could be described essentially by the same set of time constants and fractional contributions indicated re-trapping was not significant and that there was no interaction between the traps, *i.e.*, they validated the use of the superposition principle [53]. It is noted that pre-heating analysis of thermoluminescence (TL) glow curves of magnesium aluminum spinel showed evidence that broad glow peaks are composed of several superimposed glow peaks [17,47,54]. If the trap depths for TL are distributed, it is inferred that so too will be the optical trap depths for OSL. Likewise, this means that the photoionization cross-sections and, therefore, the OSL decay rates will be distributed. Consequently, the analysis of the OSL curves using a sum of exponentials should only be considered as an empirical approach to describing the OSL curve shapes and not an implication of the physical mechanisms of the optical detrapping processes.

Practical application of OSL dosimeters involve storage of the irradiation signal for relatively long times. This characteristic was evaluated in terms of fading of the OSL signal after 12 h storage in the dark as shown in Fig. 11 where OSL curves shown in black were obtained immediately after 200 s irradiation (in practice, 17 s passed between the end of irradiation and the start of the OSL measurement, a time required to rotate the sample tray from “irradiation” to

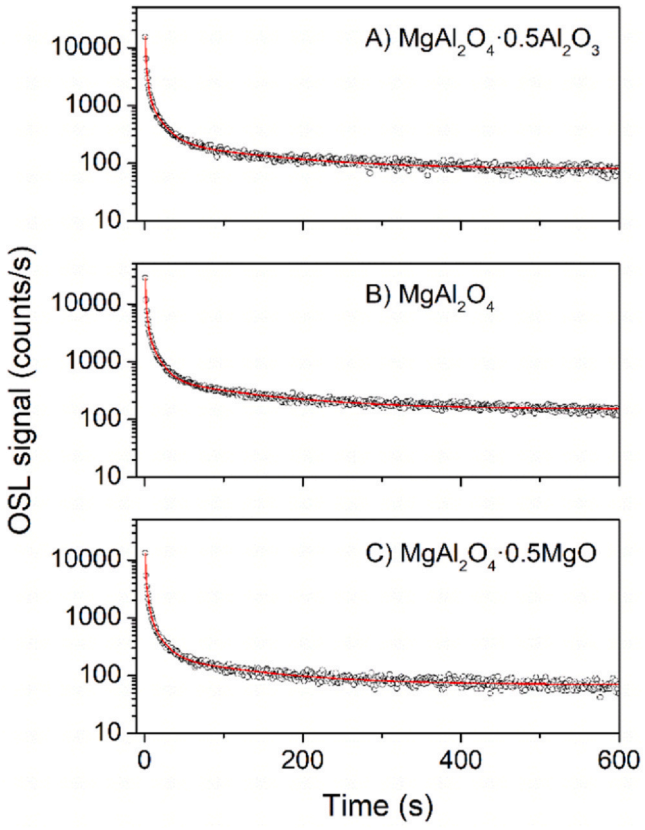

Fig. 10. OSL curves obtained after 600 s stimulation of spinels with different Mg:Al ratios (open circles) together with best fit using four exponential functions (red lines) and one free constant background. Samples were irradiated for 10 s. All figures are in the same scale to facilitate comparison.

Table 1
Minimum detectable absorbed dose (MDD) of magnesium aluminate spinel powders with different Mg:Al ratios.

Mg:Al ratio	MDD (mGy)
1.5:2	1.24
1:2	0.65
1:3	1.20

Table 3
Parameters of the analysis of OSL curve decays after 600 s stimulation for an irradiation time of 10 s. Time constants are given in seconds and their fractional contributions in percentage.

Mg:Al	Time constant (s)	Time constant (s) Fractional contribution
1:3	τ_1	0.573
	τ_1 fractional contribution	33%
	τ_2	2.61
	τ_2 fractional contribution	21%
	τ_3	14.6
	τ_3 fractional contribution	21%
	τ_4	130
	τ_4 fractional contribution	25%
1:2	τ_1	0.494
	τ_1 fractional contribution	30%
	τ_2	2.17
	τ_2 fractional contribution	21%
	τ_3	11.9
	τ_3 fractional contribution	22%
	τ_4	118
	τ_4 fractional contribution	27%
1.5:2	τ_1	0.514
	τ_1 fractional contribution	34%
	τ_2	2.77
	τ_2 fractional contribution	23%
	τ_3	13.2
	τ_3 fractional contribution	19%
	τ_4	116
	τ_4 fractional contribution	24%

"OSL readout" position in the Risø reader) and in red after 12 h storage. A similar behavior was observed for all Mg:Al ratios with the decrease of the initial signal (t = 0 s) being the least (8×) for the stoichiometric material and the highest for the Al-rich material (13×), with the decrease of the Mg-rich being 10× of the respective initial signal obtained immediately after irradiation TL fading after storage in the dark was reported in other materials. Not coincidently, those materials presented broad TL peaks and non-zero TL signal at around RT [*e.g.*, [20,55,56]]. In the case of magnesium aluminum spinel, a TL glow peak just above RT was commonly reported [43,46,57,58], and a TL peak at around 70 °C was attributed to Al_{Mg} antisite defects [17 and references therein]. While further investigation is needed to fully understand OSL fading of magnesium aluminum spinel, based on the evidence at hand, it was tentatively related to the instability of TL close to RT.

Table 2
Parameters of the analysis of OSL curve decays after 100 s stimulation for selected irradiation times. Time constants are given in seconds and their fractional contributions in percentage.

Mg:Al	Time constant (s)	Irradiation time (s)			Average time constant (s)
		10	100	200	Average fractional contribution
1:3	τ_1	0.588	0.535	0.580	0.57
	τ_1 fractional contribution	14%	11%	11%	12%
	τ_2	3.24	2.77	2.96	3.0
	τ_2 fractional contribution	36%	35%	34%	35%
	τ_3	20.5	18.0	18.9	19
	τ_3 fractional contribution	50%	54%	55%	53%
1:2	τ_1	0.543	0.562	0.578	0.56
	τ_1 fractional contribution	12%	11%	11%	11%
	τ_2	2.80	3.04	3.10	3.0
	τ_2 fractional contribution	36%	36%	35%	36%
	τ_3	17.8	18.2	18.9	18
	τ_3 fractional contribution	52%	53%	54%	53%
1.5:2	τ_1	0.585	0.604	0.593	0.59
	τ_1 fractional contribution	12%	11%	10%	11%
	τ_2	2.91	3.24	3.18	3.1
	τ_2 fractional contribution	33%	34%	34%	34%
	τ_3	18.2	19.4	19.5	19
	τ_3 fractional contribution	55%	55%	56%	56%

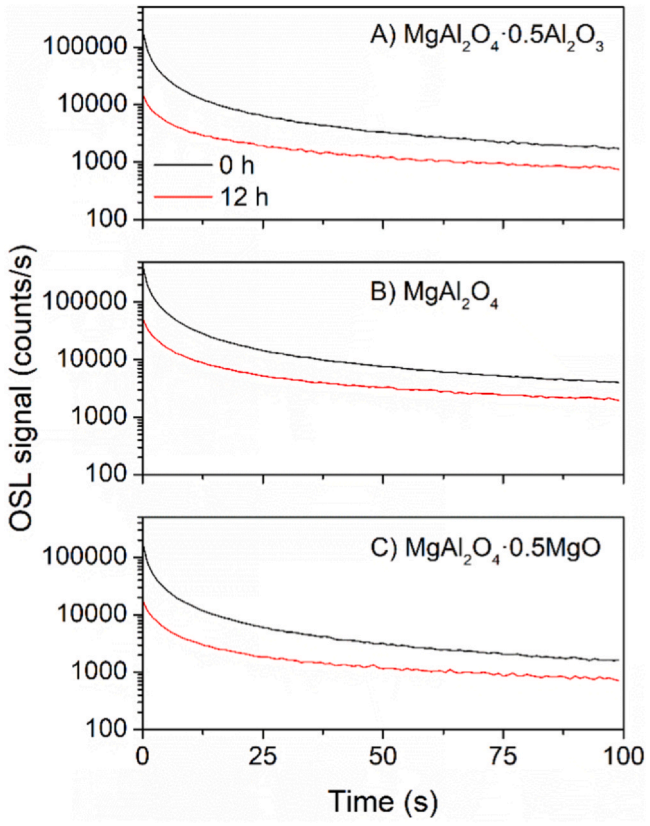

Fig. 11. Fading evaluation of the OSL signal of spinels with different Mg:Al ratios: black curves were obtained immediately after 200 s irradiation, and red curves were obtained after 12 h storage in the dark.

4. Conclusions

An investigation of the effects of the Mg:Al ratio of magnesium aluminum spinel in the luminescence, and especially in the OSL response, was performed for the first time combined with microstructural characterization. A higher level of structural disorder was found in the powders than in the single crystal, while the same luminescence centers were present in all materials. The OSL dose-response characteristics of all powders were non-linear. The non-linearity is believed to be the result of fading of the OSL signal during irradiation. The OSL signal is believed to originate from thermally unstable centers when stimulated at 470 nm at RT. For short irradiation times (over the dose range 0.16–2 Gy for the dose rate used in this experiment) the dose-response function is approximately linear, especially for stoichiometric spinel. The OSL curve shapes are consistently described by a sum of multiple, first-order, OSL decay curves. The sensitivity of stoichiometric spinel was between 1.9 and 2.2 times greater than the other two spinel samples and had the smallest MDD (0.65 mGy) with a reproducibility of ±1%.

CRediT authorship contribution statement

L. Pan: Formal analysis, Investigation, Data curation, Writing - original draft, Writing - review & editing, Visualization. **S. Sholom:** Conceptualization, Methodology, Formal analysis, Investigation, Resources, Data curation, Writing - review & editing. **S.W.S. McKeever:** Conceptualization, Methodology, Formal analysis, Investigation, Resources, Data curation, Writing - review & editing. **L.G. Jacobsohn:** Conceptualization, Methodology, Formal analysis, Investigation, Resources, Data curation, Writing - original draft, Writing - review & editing, Visualization, Supervision, Project administration, Funding acquisition.

Declaration of Competing Interest

The authors declare that they have no known competing financial interests or personal relationships that could have appeared to influence the work reported in this paper.

Acknowledgments

This material is based upon work supported by the National Science Foundation under Grant No. 1653016 to Clemson University. The work at Oklahoma State University is supported by the State of Oklahoma.

References

[1] L.S. Cain, G.J. Pogatshnik, Y. Chen, Optical transitions in neutron-irradiated $MgA1_2O_4$ spinel crystals, Phys. Rev. B 37 (1988) 2645–2652.
[2] H. Ishii, J. Hiraishi, T. Yamanaka, Structure and lattice vibrations of Mg-Al spinel solid solution, Phys. Chem. Miner. 8 (1982) 64–68.
[3] R. Dupree, M.H. Lewis, M.E. Smith, A study of the vacancy distribution in non-stoichiometric spinels by magic-angle spinning NMR, Philos. Mag. A 53 (1986) L17–L20.
[4] Cation disorder and vacancy distribution in nonstoichiometric magnesium aluminate spinel, $MgO{\cdot}xAl_2O_4$, J. Am. Ceram. Soc. 82 (1999) 3293–3298.
[5] T. Soeda, S. Matsumura, J. Hayata, C. Kinoshita, Quantitative electron diffraction study of cation configuration and irradiation induced displacement in magnesium aluminate spinel crystals, J. Electron Microsc. 48 (1999) 531–536.
[6] C.A. Gilbert, R. Smith, S.D. Kenny, S.T. Murphy, R.W. Grimes, J.A. Ball, A theoretical study of intrinsic point defects and defect clusters in magnesium aluminate spinel, J. Phys. Condens. Matter 21 (2009) 275406.
[7] R.L. Mohler, W.B. White, Influence of structural order on the luminescence of oxide spinels: manganese activated spinels, Mater. Res. Bull. 29 (1994) 1109–1116.
[8] G.P. Summers, Radiation damage in $MgAl_2O_4$, Phys. Rev. B 21 (1980) 2578–2584.
[9] A. Lushchik, S. Dolgov, E. Feldbach, R. Pareja, A.I. Popov, E. Shablonin, V. Seeman, Creation and thermal annealing of structural defects in neutron-irradiated $MgAl_2O_4$ single crystals, Nucl. Instrum. Methods Phys. Res. B 435 (2018) 31–37.
[10] E. Feldbach, I. Kudryavtseva, K. Mizohata, G. Prieditis, J. Räisänen, E. Shablonin, A. Lushchik, Optical characteristics of virgin and proton-irradiated ceramics of magnesium aluminate spinel, Opt. Mater. 96 (2019) 109308.
[11] Y. Takebuchi, H. Fukushima, T. Kato, D. Nakauchi, N. Kawaguchi, T. Yanagida, Optical, scintillation, and dosimetric properties of Mn-doped $MgAl_2O_4$ single crystals, J. Mater. Sci. Mater. Electron. 31 (2020) 8240–8247.
[12] T. Katsumata, H. Takeuchi, S. Komuro, H. Aizawa, X-ray detector based on Mn doped $MgAl_2O_4$ and Si photodiode, Rev. Sci. Instrum. 89 (2018) 095104.
[13] T. Katsumata, S. Minowa, T. Sakuma, A. Yoshida, S. Komuro, H. Aizawa, X-ray excited optical luminescence from Mn doped spinel crystals, ECS Solid State Lett. 3 (2014) R23–R25.
[14] D. Valiev, O. Khasanov, S. Stepanov, E. Dvilis, V. Paygin, $MgAl_2O_4$ ceramics doped with rare earth ions: synthesis and luminescent properties, AIP Conf. Proc. 2174 (2019) 0202625.
[15] T. Kato, D. Nakauchi, N. Kawaguchi, T. Yanagida, Thermally stimulated luminescence properties of Tm-doped $MgAl_2O_4$ transparent ceramics, Opt. Mater. 106 (2020) 110028.
[16] T. Kato, D. Nakauchi, N. Kawaguchi, T. Yanagida, Optical, scintillation, and dosimetric properties of Dy-doped $MgAl_2O_4$ transparent ceramics, Optik 207 (2020) 164433.
[17] E.M. Yoshimura, E.G. Yukihara, Optically stimulated luminescence of magnesium aluminate ($MgAl_2O_4$) spinel, Radiat. Meas. 41 (2006) 163–169.
[18] M.W. Blair, L.G. Jacobsohn, S.C. Tornga, O. Ugurlu, B.L. Bennett, E.G. Yukihara, R.E. Muenchausen, Nanophosphor aluminum oxide: luminescence response of a potential dosimetric material, J. Lumin. 130 (2010) 825–831.
[19] J.R. Hazelton, E.G. Yukihara, L.G. Jacobsohn, M.W. Blair, R. Muenchausen, Feasibility of using oxyorthosilicates as optically stimulated luminescence detectors, Radiat. Meas. 45 (2010) 681–683.
[20] E.G. Yukihara, E.D. Milliken, L.C. Oliveira, V.R. Orante-Barrón, L.G. Jacobsohn, M.W. Blair, Systematic development of new thermoluminescence and optically stimulated luminescence materials, J. Lumin. 133 (2013) 203–210.
[21] T.D. Gustafson, E.D. Milliken, L.G. Jacobsohn, E.G. Yukihara, Progress and challenges towards the development of a new optically stimulated luminescence (OSL) material based on MgB_4O_7:Ce,Li, J. Lumin. 212 (2019) 242–249.

[22] A.J.J. Bos, High sensitivity thermoluminescence dosimetry, Nucl. Instrum. Methods Phys. Res. B 184 (2001) 3–28.
[23] E. Alagu Raja, Sanjeev Menon, Bhushan Dhabekar, N.S. Rawat, T.K. Gundu Rao, Investigation of defect centres responsible for TL/OSL in $MgAl_2O_4$:Tb^{3+}, J. Lumin. 129 (2009) 829–835.
[24] Sanu S. Raj, D.R. Mishra, Anuj Soni, V. Grover, G.S. Polymeris, K.P. Muthe, S.K. Jha, A.K. Tyagi, TL and OSL studies of carbon doped magnesium aluminate ($MgAl_2O_4$:C), Radiat. Phys. Chem. 127 (2016) 78–84.
[25] Y. Takebuchi, H. Fukushima, D. Nakauchi, T. Kato, N. Kawaguchi, T. Yanagida, Scintillation and dosimetric properties of Ce-doped $MgAl_2O_4$ single crystals, J. Lumin. 223 (2020) 117139.
[26] T. Kato, Y. Takebuchi, D. Nakauchi, N. Kawaguchi, T. Yanagida, Dosimetric properties of undoped and Tb-doped $MgAl_2O_4$ transparent ceramics, Radiat. Meas. 135 (2020) 106341.
[27] D. Richter, A. Richter, K. Dornich, Lexsyg – a new system for luminescence research, Geochron 40 (2013) 220–228.
[28] J.R. Lakowicz, Principles of Fluorescence Spectroscopy, 3rd ed., Springer, New York, 2006 chap. 4.
[29] L.M. Fraas, J.E. Moore, J.B. Salzberg, Raman characterization studies of synthetic and natural $MgAl_2O_4$ crystals, J. Chem. Phys. 58 (1973) 3585–3592.
[30] A. Chopelas, A.M. Hofmeister, Vibrational spectroscopy of aluminate spinels at 1 atm and of $MgAl_2O_4$ to over 200 kbar, Phys. Chem. Miner. 18 (1991) 279–293.
[31] H. Cynn, S.K. Sharma, T.F. Cooney, M. Nicol, High-temperature Raman investigation of order-disorder behavior in the $MgAl_2O_4$ spinel, Phys. Rev. B 45 (1992) 500–502.
[32] M. Lazzeri, P. Thibaudeau, Ab initio Raman spectrum of the normal and disordered $MgAl_2O_4$ spinel, Phys. Rev. B 74 (2006) 140301.
[33] V.T. Gritsyna, I.V. Afanasyev-Charkin, V.A. Kobyakov, Structure and electronic states of defects in spinel of different compositions $MgO{\cdot}nAl_2O_3$:Me, J. Am. Ceram. Soc. 82 (1999) 3365–3373.
[34] A. Tomita, T. Sato, K. Tanaka, Y. Kawabea, M. Shirai, K. Tanaka, E. Hanamura, Luminescence channels of manganese-doped spinel, J. Lumin. 109 (2004) 19–24.
[35] K. Izumi, T. Mizokawa, E. Hanamura, Optical response and electronic structure of Zn-doped $MgAl_2O_4$, J. Appl. Phys. 102 (2007) 053109.
[36] T. Sakuma, S. Minowa, T. Katsumata, S. Komuro, H. Aizawa, Compositional variation of photoluminescence from Mn doped $MgAl_2O_4$ spinel, Opt. Mater. 37 (2014) 302–305.
[37] A. Ibarra, D.F. Mariani, M. Jimenez de Castro, Thermoluminescent processes of $MgAl_2O_4$ irradiated at room temperature, Phys. Rev. B 44 (1991) 12158–12165.
[38] J.M.G. Tijero, A. Ibarra, Use of luminescence of Mn^{2+} and Cr^{3+} in probing the disordering process in $MgAl_2O_4$ spinels, J. Phys. Chem. Solids 54 (1993) 203–207.
[39] P.K. Bandyopadhyay, G.P. Summers, Luminescence and photoconductivity in magnesium aluminum spinel, Phys. Rev. B 31 (1985) 2422–2426.
[40] J.M. Bunch, Mollwo-Ivey relation between peak color-center absorption energy and average oxygen ion spacing in several oxides of group-II and -III metals, Phys. Rev. B 16 (1977) 724–725.
[41] S. White, K.H. Lee, J.H. Crawford, Thermochemical coloration and annealing of spinel and magnesium oxide, Appl. Phys. Lett. 35 (1979) 1–3.
[42] S. Sawai, T. Uchino, Visible photoluminescence from $MgAl_2O_4$ spinel with cation disorder and oxygen vacancy, J. Appl. Phys. 112 (2012) 103523.
[43] A. Ibarra, M. Jimenez de Castro, Thermoluminescence in $MgAl_2O_4$ X-ray irradiated at 90 K, J. Phys. Chem. Solids 53 (1992) 1191–1198.
[44] S.V. Motloung, F.B. Dejene, M.E. Sithole, L.F. Koao, O.M. Ntwaeaborwa, H.C. Swart, T.E. Motaung, The effects of Cd^{2+} concentration on the structure, optical and luminescence properties of $MgAl_2O_4$:x% Cd^{2+} ($0 < x < 1.75$) nanophosphor prepared by sol-gel method, J. Electron. Mater. 45 (2016) 4796–4805.
[45] I. Jozwik, J. Jagielski, G. Gawlik, P. Jozwik, R. Ratajczak, G. Panczer, N. Moncoffre, A. Wajler, A. Sidorowicz, L. Thomé, Comparative study of radiation-induced damage in magnesium aluminate spinel by means of IL, CL and RBS/C techniques, Phys. Chem. Miner. 43 (2016) 439–445.
[46] V.T. Gritsyna, Yu.G. Kazarinov, V.A. Kobyakov, I.E. Reimanis, Radiation-induced luminescence in magnesium aluminate spinel crystals and ceramics, Nucl. Instrum. Methods Phys. Res. B 250 (2006) 342–348.
[47] A. Lorincz, M. Puma, F.J. James, J.H. Crawford, Thermally stimulated processes involving defects in γ- and x-irradiated spinel ($MgAl_2O_4$), J. Appl. Phys. 53 (1982) 927–932.
[48] O.K. Tyutyunik, A.O. Moskvitin, Yu.G. Kazarinov, V.T. Gritsyna, Radioluminescence mechanism of magnesium aluminate spinel transparent ceramics, Funct. Mater. 17 (2010) 41–45.
[49] V. Gritsyna, Y. Kazarinov, Effects of transition-metal-doping on the radio-luminescence properties of magnesium aluminate spinel crystals, Radiat. Appl. 3 (2018) 7–12.
[50] M. Tamatani, Principal phosphor materials and their optical properties, in: W.M. Yen, S. Shionoya, H. Yamamoto (Eds.), Fundamentals of Phosphors, CRC Press, Boca Raton, 2007, p. 173.
[51] T. Kato, G. Okada, T. Yanagida, Optical, scintillation and dosimeter properties of MgO transparent ceramic doped with Mn^{2+}, J. Ceram. Soc. Jpn. 124 (2016) 559–563.
[52] V.T. Gritsyna, I.V. Afanasyev-Charkin, Yu.G. Kazarinov, K.E. Sickafus, Optical properties of magnesium aluminate spinel crystals implanted with helium ions, Vacuum 81 (2006) 174–178.
[53] L. Botter-Jensen, S.W.S. McKeever, A.G. Wintle, Optically Stimulated Luminescence Dosimetry, Elsevier, Amsterdam, 2003 chap. 2.
[54] T.K. Kim, H.S. Choe, J.I. Lee, C.N. Whang, Thermoluminescence spectra of $MgAl_2O_4$ irradiated with X-rays, J. Korean Phys. Soc. 30 (1997) 347–351.
[55] L.G. Jacobsohn, A.L. Roy, C.L. McPherson, C.J. Kucera, L.C. Oliveira, E.G. Yukihara, J. Ballato, Rare earth-doped nanocrystalline MgF_2: synthesis, luminescence and thermoluminescence, Opt. Mater. 35 (2013) 2461–2464.
[56] N.M. Trindade, M.R. da Cruz, H. Kahn, L.G. Jacobsohn, E.M. Yoshimura, Thermoluminescence and radioluminescence of alexandrite mineral, J. Lumin. 206 (2019) 455–461.
[57] D. Jia, W.M. Yen, Enhanced $V_K{}^{3+}$ center afterglow in $MgAl_2O_4$ by doping with Ce^{3+}, J. Lumin. 101 (2003) 115–121.
[58] G. Prieditis, E. Feldbach, I. Kudryavtseva, A.I. Popov, E. Shablonin, A. Lushchik, IOP Conf. Ser. Mater. Sci. Eng. 503 (2019) 0120217.